ORIGINAL PAPER

Anodic alumina membranes with defined pore diameters and thicknesses obtained by adjusting the anodizing duration and pore opening/widening time

Leszek Zaraska · Grzegorz D. Sulka · Marian Jaskuła

Abstract The through-hole porous anodic aluminum oxide (AAO) membranes were fabricated by a simple two-step anodization of aluminum in 0.3 M oxalic acid, 0.3 M sulfuric acid, and 2 wt.% phosphoric acid solutions under different operating conditions followed by the removal of the remaining Al substrate and the pore opening/widening process. The effect of duration of the second anodizing step on the thickness of the porous oxide layer and the influence of other anodizing conditions such as applied voltage, type of electrolyte, and purity of the substrate on the rate of porous oxide growth were discussed in detail. The pore opening procedure for all synthesized membranes was optimized, and the influence of the duration of chemical etching on structural features of AAO membranes, especially pore diameter, was studied. The rate of pore widening was established for AAO membranes formed in various anodizing electrolytes and for different temperatures of 5 wt.% H_3PO_4 used for alumina dissolution.

Keywords Anodization · Porous alumina · Pore widening · Nanoporous materials

Introduction

Recently, a great scientific interest has been focused on all aspects of nanoscience and nanotechnology that have the potential to produce novel materials and devices with tremendous improvement in performance and reliability,

L. Zaraska (✉) · G. D. Sulka · M. Jaskuła
Department of Physical Chemistry and Electrochemistry,
Faculty of Chemistry, Jagiellonian University,
Ingardena 3,
30–060 Krakow, Poland
e-mail: zaraska@chemia.uj.edu.pl

and at substantially lower cost. Many research groups have been intensively working on fabrication of various nanostructured materials that can offer unique properties and open a lot of new perspectives in almost all disciplines [1]. Considerable attention is given to an inexpensive fabrication of periodically ordered nanomaterials such as nanowire [2–4], nanotube [5, 6], and nanopore arrays [7]. Over the last decade, many interesting strategies for nanofabrication have been proposed. Among them, template-assisted methods seem to be the most popular approaches for fabricating one-dimensional materials such as nanowires and nanotubes [8, 9].

Nanoporous anodic aluminum oxide (AAO) with hexagonally arranged pores, which have the diameter from tens to few hundred of nanometers, and with the thickness up to 100 μm can be easily fabricated by a simple two-step anodization of aluminum in acidic electrolytes [10, 11]. The process results in the formation of the porous alumina layer that consists of hexagonal cells with nanopores at their centers. At the bottom of pores, a continuous and dielectric oxide layer, called barrier layer, is built [12]. The simplicity and low cost of this procedure make AAO membranes one of the most popular template materials used for nanofabrication [13]. A great number of reports on the AAO template-assisted fabrication of metallic, semiconductor, polymeric, organic and inorganic nanomaterials such as nanowires, nanotubes, nanodots, and nanoporous structures have been published during the last few years [13]. A primary advantage of nanoporous AAO templates is the fact that all structural features of the templates, including pore diameter, interpore distance, barrier layer thickness, and oxide layer thickness, etc., can be easily tailored to desired values by adjusting anodizing conditions, especially applied voltage, process duration, and the type and concentration of the electrolyte [12]. Nowadays, in most

cases, nanoporous AAO membranes are fabricated by a voltage-controlled two-step anodization performed in sulfuric acid [14–16], oxalic acid [17, 18], and phosphoric acid [19, 20] solutions. It is widely recognized that the best nanopore order in self-organized AAOs is observed at a certain value of the anodizing voltage that is different for each electrolyte. For anodizing carried out in sulfuric acid, oxalic acid, and phosphoric acid, this voltage is exactly 25 V, 40 V, and 195 V, respectively [12].

The characteristic parameters of AAO templates such as pore diameter, interpore distance, "barrier layer" thickness, and rate of oxide growth are strongly dependent on applied voltage [12]. It is widely recognized that both the pore diameter and the interpore distance are linearly proportional to the anodizing potential with proportionality constants of about 1.29 nm V^{-1} [21] and 2.5 nm V^{-1} [22], respectively. On the other hand, the pore diameter does not change significantly with increasing anodizing time. For a very long process, a small widening of pores can be observed especially near the oxide/electrolyte interface. This fact can be attributed to an extended contact of oxide with an acidic electrolyte and the effect of field-enhanced dissolution of Al_2O_3 [23]. Other factors that might have an influence on the pore diameter are: the electrolyte concentration (a more acidic electrolyte is used for anodizing larger pore diameter is observed), temperature (increasing temperature increases pore diameter), and even a solution stirring speed [12]. The effect of anodizing temperature on the interpore distance depends on the type of anodizing electrolyte used. In case when anodizations are carried out in oxalic acid, the dependence between the interpore distance and anodizing temperature is almost negligible [24]. For sulfuric acid used as an electrolyte, increasing temperature results in an increase in the interpore distance [16]. On the other hand, the barrier layer thickness depends not only on the applied potential but also on other conditions such as a type of electrolyte and the process duration. Therefore, the anodizing ratio, defined as a barrier layer thickness per volt, varies from 0.8 to 1.15 nm V^{-1} [12]. Summing up, the structural features of AAO templates can be fine-tuned by changing the anodization voltage. Moreover, the pore diameter can be easily enlarged by post-anodizing etching of formed oxide.

In order to obtain a through-hole nanoporous AAO membrane with a certain pore diameter, usually posttreatment procedures are applied including a wet-chemical route to the selective and uniform removal of the remaining Al substrate followed by etching of the barrier layer. The pore opening process can be performed using a dry etching with an Ar^+ ion beam [25–28], Ga^+ ion beam [29, 30], BCl_3 reactive ions [31], and CF_4 reactive ions [32]. Although the dry etching process is capable of removing the barrier layer on a selected surface area (opening of even single pore), the

technique requires an expensive and sophisticated equipment. Therefore, the most widespread method used for the opening of pores is a wet chemical etching usually carried out in a phosphoric acid solution [24, 33, 34]. It is worth to emphasize that the rate of chemical etching of the barrier layer depends especially on the electrolyte concentration and temperature. That is why the procedure of barrier layer removal should be carefully optimized [12]. The process of pore opening and widening was studied by Xu et al. [33] for samples anodized in 0.3 M $H_2C_2O_4$ at 40 V and 12 °C. The rate of dissolution of the barrier layer in 5 wt.% H_3PO_4 and 30 °C was estimated to be approximately 1.3 nm min^{-1}. It was found that the dissolution rate decreases inside the pore channel with increasing the depth of pores. The authors proposed inhomogeneous dissolution of alumina and distinguished horizontal and vertical dissolution rates. The first one is mainly responsible for the barrier layer removal, whereas the vertical rate plays a key role in the widening of pores.

In this work, we presented some results on fabrication of through-hole nanoporous AAO membranes with various pore diameters. We focused our attention on optimization of the second anodizing step duration and determination of the oxide growth rate under different conditions. Additionally, the pore opening/widening procedure is discussed in detail for AAO membranes formed by two-step anodization of the high-purity Al foil carried out in different anodizing electrolytes and different anodizing potentials. For dissolution performed in 5 wt.% phosphoric acid at various temperatures, the vertical dissolution rates (pore widening rates) were estimated for AAO membranes formed in different electrolytes and anodizing potentials.

Experimental

A high-purity aluminum foil (0.5-mm thick, 99.999% in purity, Goodfellow) as well as commercially available AA1050 alloy were used as starting materials. The composition of AA1050 was minimum of 99.5% Al with Fe <0.30% and Si <0.2% as principal alloying elements. The substrates were cut into specimens with dimensions of 25×5×0.5 mm. A two-step anodizing procedure was used for the generation of self-ordered nanoporous AAO membranes. The experimental procedure is schematically shown in Fig. 1.

At first, samples were degreased in acetone and ethanol. Then, the electrochemical polishing was performed in a mixture of perchloric acid (60 wt.%) and ethanol (1:4 vol.) under the constant current density of 0.5 A cm^{-2} or constant voltage of 20 V for 1 min at 10 °C (Fig. 1a). The oxide layer formed on the Al surface during the first anodization (Fig. 1b) was chemically removed by immersing in a
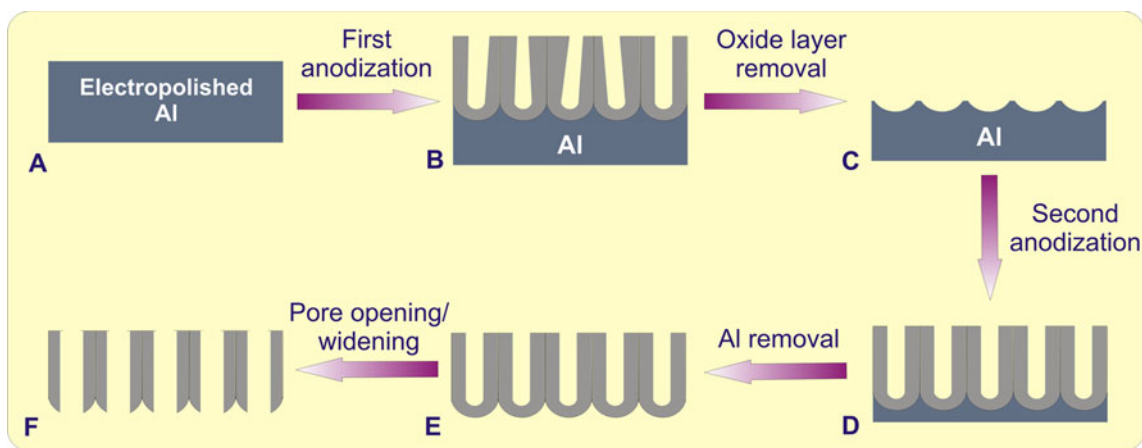
Fig. 1 A schematic representation of the experimental procedure

mixture of 6 wt.% H_3PO_4 and 1.8 wt.% H_2CrO_4 at 45 °C for 12 h (Fig. 1c). After that, the second anodization was performed under the same conditions as were used in the first electrolysis (Fig. 1d). The anodizing conditions used for fabrication of AAO membranes are collected in Table 1.

The remaining Al substrate was removed by immersing the specimen in a saturated $HgCl_2$ solution (Fig. 1e). After degreasing in ethanol, a chemical etching of the barrier layer at the pore bottoms was performed in H_3PO_4 solution. The AAO membrane was put on a microscopic slide glass, dipped into a non-stirred solution, and kept in a water bath for a specified period of time. The top layer of the oxide membranes adhered to the microscopic slide glass, and the bottom side of membranes was exposed to the acidic solution. By monitoring the duration of the pore opening process, membranes with a different pore diameter were obtained (Fig. 1f). The operating conditions used for pore opening/widening are collected in Table 1. After the pore opening, AAO membranes were cleaned in water and ethanol and dried. The sample morphology was determined with a field-emission scanning electron microscope (FE-SEM. Hitachi S-4700). The structural features of AAO membranes such as oxide layer thickness (Θ), interpore distance (D_c), and pore diameter (D_p) were calculated on the basis of FE-SEM images by using the scanning probe image processor WSxM v. 12.0 [35] and ImageJ software [36]. The pore density (ρ) and porosity of membranes (σ) were calculated from the well-known equations [12]:

$$\rho = \frac{2 \times 10^{14}}{\sqrt{3} \times D_c^2} \qquad (1)$$

$$\sigma = \frac{\pi}{2\sqrt{3}} \times \left(\frac{D_p}{D_c}\right)^2 = 0.907 \times \left(\frac{D_p}{D_c}\right)^2 \qquad (2)$$

Results and discussion

In order to obtain nanoporous AAO membrane with a precisely controlled thickness of the oxide layer, the adjustment of second anodizing step duration is a very important issue. In general, the rate of oxide growth depends mainly on the type of electrolyte and its concentration, anodizing voltage, temperature of the process, as well as on the type of starting material. The two-step anodizing experiments were carried out under different conditions with the purpose of studying the influence of the anodizing parameters on the rate of oxide growth. The dependence of the oxide layer thickness on the duration of the second anodizing step is shown in Fig. 2 for various operating conditions and starting materials.

In all cases, strong linear relationships between the thickness of oxide layer and anodizing time were obtained. The calculated rates of oxide growth are collected in Table 2.

It is clearly seen that the rate of oxide growth depends on the type of electrolyte for processes carried out at similar temperatures. For the high-purity Al foil used as a starting material, the highest rate was observed for the anodization performed in a sulfuric acid solution. A slight decrease in the rate of oxide growth was recorded when the anodization was carried out in oxalic acid, and the lowest growth rate was observed in a phosphoric acid solution. When the AA150 alloy is used as a starting material, the oxide growth rates are significantly smaller, as can be seen in Table 2. The causes of this phenomenon were described in our previous works [37].

On the other hand, the oxide growth rate increases considerably with increasing anodizing temperature. For instance, the oxide growth rates for anodizations performed in oxalic acid at 20 °C are almost seven times higher than the growth rates at 1 °C. This is a significant advantage from the economical point of view because the higher

Table 1 All experimental parameters together with characteristic parameters of as-obtained nanoporous alumina membranes

| Starting material | Fabrication of nanoporous membranes | | | | | | | Characteristic parameters of AAO | | | | | Pore widening rate [nm min^{-1}] |
| | Anodization | | | | Pore opening/widening | | | | | | | | |
	Electrolyte	U [V]	t_1/t_2 [h]	T [°C]	Electrolyte	T [°C]	t_o [min]	Θ [µm]	D_c [nm]	D_p [nm]	ρ [cm^{-2}]	σ [%]	
Al 99.999%	0.3 M H$_2$SO$_4$	25	8/10	1	5 wt.% H$_3$PO$_4$	30	24	~40	59	24	3.32 10^{10}	15.0	3.03
Al 99.999%	0.3 M H$_2$C$_2$O$_4$	40	8/16	1	5 wt.% H$_3$PO$_4$	25	90	~30	91	70	1.39 10^{10}	53.7	n.a.
Al 99.999%	0.3 M H$_2$C$_2$O$_4$	45	1/4	20	5 wt.% H$_3$PO$_4$	25	90	~50	107	76	1.01 10^{10}	45.8	0.80
Al 99.999%	0.3 M H$_2$C$_2$O$_4$	45	1/4	20	5 wt.% H$_3$PO$_4$	35	50	~50	107	31	1.01 10^{10}	7.6	0.55 (top of the membrane) 1.02 (bottom of the membrane)
AA1050	0.3 M H$_2$C$_2$O$_4$	45	1/4	20	5 wt.% H$_3$PO$_4$	25	90	~35	94	44	1.31 10^{10}	19.9	0.43
Al 99.999%	0.3 M H$_2$C$_2$O$_4$	60	1/2	20	5 wt.% H$_3$PO$_4$	45	45	~50	168	72	4.09 10^{9}	16.7	1.22 (top of the membrane) 2.23 (bottom of the membrane)
Al 99.999%	2 wt.% H$_3$PO$_4$ in methanol/water system (1:4 vol.)	175	8/30	0	10 wt.% H$_3$PO$_4$	45	50	~55	414	244	6.74 10^{8}	31.5	n.a.

U anodizing voltage, t_1/t_2 duration of the first/second anodizing step, T temperature, t_o pore opening/widening time, Θ oxide layer thickness, D_c interpore distance (cell diameter), D_p pore diameter measured at the bottom side of the membrane, ρ pore density, σ porosity

temperature of the process causes faster production of thick AAO membranes and lower costs of investment and power consumption for cooling. Since AAO membranes are often used as hard templates for synthesis of nanostructured materials, the regularity of nanohole arrangement is also an important aspect for anodizing process optimization. A similar, high degree of pore order within the AAO membranes was observed independently of anodizing temperature [18, 38]. Our previous result showed that AAO membranes with a satisfying pore order degree can be fabricated also at the temperature of 20 °C.

Another important parameter is anodizing voltage. For the process carried out in 0.3 M oxalic acid at 20 °C, an increase in the applied voltage from 45 to 60 V results in a significant increase of the oxide growth rate of about 9 µm h^{-1} (Table 2). Simultaneously, it should be mentioned that increasing applied voltage increases the pore diameter and interpore distance (see Table 1) as well as deteriorates the regularity of nanopore arrangement (the best nanopore arrangement for anodization carried out in oxalic acid is around 40–45 V) [17].
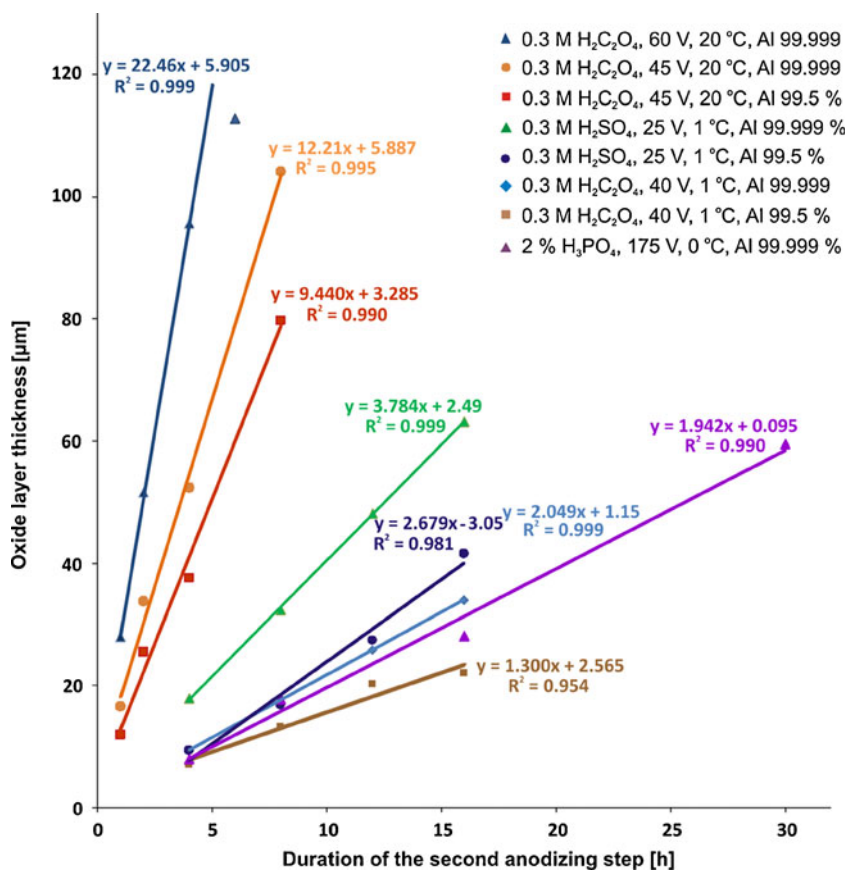
As can be seen in Table 2, the oxide growth rate decreases in most cases with increasing duration of the process. This behavior can be explained by the diffusion-limited electrochemical oxidation of aluminum at the pore bottoms. It is widely recognized that nanoporous Al$_2$O$_3$ is electrochemically formed at the metal/oxide interface [12]. For the extended anodization, the built oxide layer is thick, and the time required for diffusion of reactant species over the whole pore length is much longer. So, when the nanoporous layer grows, the diffusion of electrolyte to the pore bottoms becomes more difficult, and the process of oxide formation slows down.

The as-prepared nanoporous AAO membrane, after the removal of remaining Al substrate, has still closed pore bottoms due to the presence of continuous barrier layer. Therefore, the last step of through-hole membrane preparation is a pore opening/widening carried out in a phosphoric acid solution. It should be mentioned that the thickness of barrier layer is not the same for all AAO membranes and depends on the type of electrolyte and anodizing conditions, especially applied voltage. Moreover, the etching rate of AAO strongly depends on the concentration of H$_3$PO$_4$ and the process temperature.

Figure 3 shows the FE-SEM images of the bottom side of AAO membranes formed by anodizing of the high-purity Al foil in 0.3 M sulfuric acid at 25 V and 1 °C. The duration of the first and second anodizing step was 8 and 10 h, respectively. The pore opening procedure was carried out in 5 wt.% H$_3$PO$_4$ at 30 °C.

It is clearly visible that after 16 min of pore opening, pores are still closed (Fig. 3a). After 20 min, the barrier layer is removed, and the diameter of pores, calculated on

the basis of FE-SEM images, is about 12 nm (Fig. 3b). When the duration of the pore opening/widening process is extended to 24 min, the average pore diameter increases to about 24 nm (Fig. 3c). The dissolution of alumina occurring in the vertical direction, being the pore widening rate estimated for already opened pores, was calculated for anodization performed in 0.3 M H_2SO_4, and obtained value is shown in Table 1.

The pore opening/widening procedure for AAO membranes formed by two-step anodizing in oxalic acid at 45 V and 20 °C was investigated for both substrates, high-purity Al and AA1050 alloy, in our previous work [38]. The pore opening/widening process was carried out in 5 wt.% H_3PO_4 at 20 °C. It was found that the rate of oxide etching was lower for membranes synthesized from the AA1050 alloy than for those fabricated by anodizing of the high-purity substrate. This was attributed to the accumulation of alloying elements, especially silicon species, in the barrier layer [38]. In general, the rate of oxide wet etching depends considerably on the temperature of the process. For AAO membranes formed by anodizing of the high-purity Al in 0.3 M $H_2C_2O_4$ at 45 V, an increase in the temperature of the pore opening process from 25 °C to 35 °C allows a significant reduction of the time required for a complete removal of the barrier layer. The pore widening rates were

also estimated for anodizations performed in 0.3 M $H_2C_2O_4$ at various experimental conditions and collected in Table 1. The different rates of pore widening estimated at the pore bottoms and mouths for samples anodized in oxalic acid are attributed to the different contents of oxalic anions incorporated in the oxide film [12]. The average pore diameter as calculated from the bottom side of AAO membranes formed by anodizing in 0.3 M oxalic acid at 45 V and 20 °C for different durations of the pore opening is shown in Fig. 4a (red line).

After 30 min of the pore opening performed in 5 wt.% H_3PO_4 at 35 °C, the pore diameter was estimated to be about 14 nm, while still closed pores were observed even after 40 min of pore opening carried out at 20 °C [18]. Figure 5 shows the FE-SEM images taken from the bottom side of the AAO membranes, fabricated by two-step anodization of the high-purity Al substrate in 0.3 M oxalic acid at 60 V and 20 °C, after different durations of the pore opening/widening. The pore opening was carried out in 5 wt.% H_3PO_4 at 45 °C. The dependence between pore diameter and duration of the chemical etching is illustrated in Fig. 4b (red line).

All the values of the average pore diameter discussed before were calculated by the ImageJ software on the basis of FE-SEM images taken from the bottom side of AAO

**Table 2** Nanoporous oxide growth rates for different anodizing conditions

Electrolyte	U [V]	T [°C]	Starting material	t_2 [h]	V_{ox} [μm h^{-1}]	V_{ox}^{av} [μm h^{-1}]
0.3 M H$_2$C$_2$O$_4$	40	1	Al 99.999%	4	2.3±0.02	2.20±0.08
				8	2.22±0.01	
				12	2.14±0.01	
				16	2.12±0.02	
0.3 M H$_2$C$_2$O$_4$	40	1	AA1050	4	1.75±0.03	1.61±0.15
				8	1.64±0.01	
				12	1.68±0.01	
				16	1.38±0.01	
0.3 M H$_2$C$_2$O$_4$	45	20	Al 99.999%	1	16.5±0.1	14.87±1.91
				2	16.88±0.08	
				4	13.09±0.32	
				8	13.02±0.1	
0.3 M H$_2$C$_2$O$_4$	45	20	AA1050	1	11.83±0.04	10.83±1.36
				2	12.74±0.05	
				4	9.41±0.05	
				8	9.97±0.05	
0.3 M H$_2$C$_2$O$_4$	60	20	Al 99.999%	1	27.87±0.35	23.93±3.64
				2	25.80±0.07	
				4	23.88±0.03	
				6	18.8±0.03	
0.3 M H$_2$SO$_4$	25	1	Al 99.999%	4	4.47±0.02	4.11±0.22
				8	4.04±0.04	
				12	4.01±0.03	
				16	3.94±0.02	
0.3 M H$_2$SO$_4$	25	1	AA1050	4	2.33±0.02	2.32±0.19
				8	2.10±0.03	
				12	2.29±0.02	
				16	2.59±0.02	
2 wt.% H$_3$PO$_4$ in methanol/ water system (1:4 vol)	175	0	Al 99.999%	4	1.96±0.01	1.87±0.26
				8	2.21±0.03	
				16	1.76±0.01	
				30	1.98±0.02	

U anodizing voltage, T temperature, t_2 duration of the second anodizing step, V_{ox} oxide growth rate, V_{ox}^{av} average oxide growth rate

membranes. Notice, importantly, that just after the second anodizing step, nanochannels in AAO membrane have their own starting diameter that increases during the pore opening process. To illustrate this effect, we calculated also the average pore diameter from the FE-SEM top-view images of AAO membranes. The relationships between the pore diameter calculated from the top side of AAO membranes and duration of the pore opening process are shown in Fig. 4a (blue line) and b (blue line) for samples anodized in 0.3 M oxalic acid at 20 °C under 45 V and 60 V, respectively. As can be seen, the wet etching of the barrier layer carried out in a phosphoric acid solution widens also the mouth of nanopores. At the top side of the AAO membrane, the rate of chemical etching is slightly lower than at the bottom side due to the adhesion of the top side of the membrane to the microscopic glass. The bottom side

of the AAO membrane is directly exposed to the etching solution. Therefore, the pore diameter at the top side of AAO widens slower than that at the bottom side. This is the reason why the duration of the pore opening/ widening process should be carefully optimized. If the immersing time is too long, the pore structure at the top side of the AAO membrane might be completely damaged by an acidic solution. At the same time, the bottom side of the membrane could be still well ordered. The problem is illustrated in Fig. 6, which shows the FE-SEM image of the top side of the AAO membrane formed by anodizing in sulfuric acid after 30 min of pore opening process.

The FE-SEM images of the bottom side of the AAO membranes formed by two-step anodization of the high-purity Al substrate in 2 wt.% H$_3$PO$_4$ at 175 V and 0 °C are

Fig. 3 FE-SEM images of the bottom side of AAO membranes formed by two-step anodizing of the high-purity Al specimens in sulfuric acid at 25 V and 1 °C. The pore opening was performed in 5 wt.% H_3PO_4 at 30 °C for 16 min (**a**), 20 min (**b**), and 24 min (**c**)
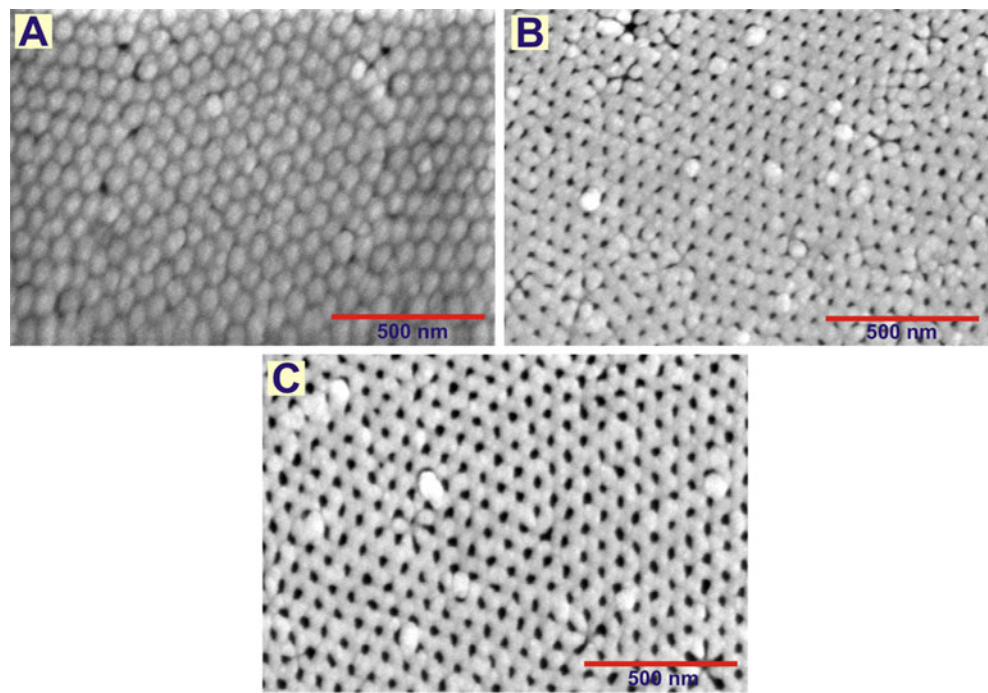
shown in Fig. 7 for different pore opening/widening durations. The porous AAO membranes, synthesized by anodizing in phosphoric acid, exhibit the thickest barrier layer among the studied samples. Therefore, the pore opening/widening process was carried out in 10 wt.% H_3PO_4 at 45 °C.

As can be seen, after 30 min of pore opening, the bottom side of the AAO membrane is still closed. Only a few holes appeared at the centers of defects that are surrounded by non-hexagonally arranged pores (Fig. 7a). After 40 min, some pores become opened but, most of them are still closed (Fig. 7b). The through-hole AAO membrane with completely opened pores and the average pore diameter of about 244 nm is obtained after 50 min of chemical etching (Fig. 7c). An interesting question may arise from the fact that we applied for anodization in phosphoric acid the

potential of 175 V instead of a well-known self-ordering regime of 195 V, at which the best pore arrangement in AAO is observed [12]. Unfortunately, in many cases, rising potential above 160 V causes active dissolution of aluminum instead of stable growth of the porous oxide film. In our previous work, we proposed a strategy for fabrication of AAO membranes with a satisfying hexagonal arrangement at lower potentials (e.g., 175 V) by using an aqueous electrolyte with a methanol content [19].

As we mentioned before, the structural features of through-hole AAO membranes such as: pore diameter, interpore distance, pore density (number of pores per 1 cm^2), and porosity were calculated for the samples anodized at different conditions and collected in Table 1. The dependences between interpore distance, pore density, and anodizing voltage for samples fabricated in different electrolytes are

Fig. 4 The dependence between pore diameter and duration of the pore opening/widening for AAO membranes obtained by two-step anodization in 0.3 M oxalic acid at 20 °C under 45 V (**a**) and 60 V (**b**). The pore opening/widening was carried out in 5 wt.% H_3PO_4 at 35 °C (**a**) and 45 °C (**b**)
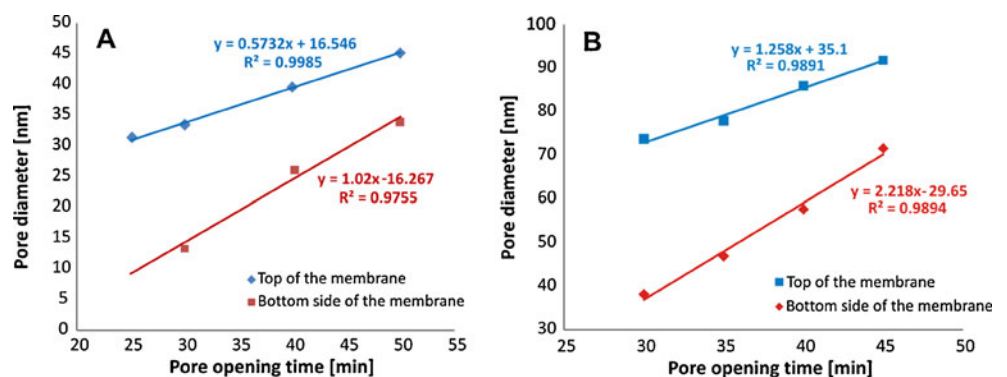
Fig. 5 FE-SEM images of the bottom sides of the AAO membranes fabricated by anodizing of the high-purity Al substrate in 0.3 M oxalic acid at 60 V and 20 °C after the pore opening/widening carried out in 5 wt.% H_3PO_4 at 45 °C. The duration of the pore opening was 20 min (**a**), 30 min (**b**), 35 min (**c**), 40 min (**d**), and 45 min (**e**)
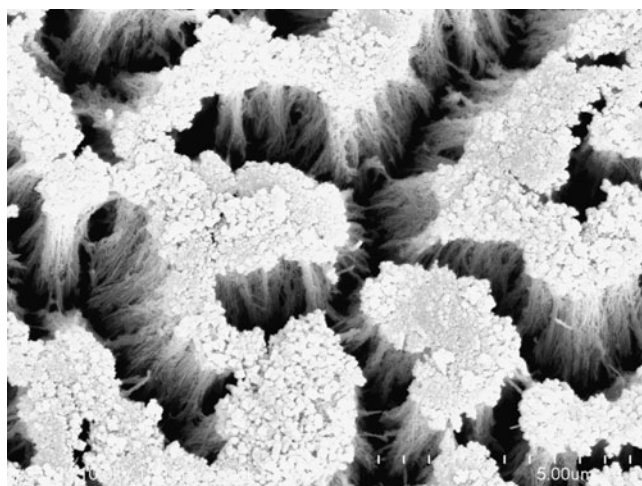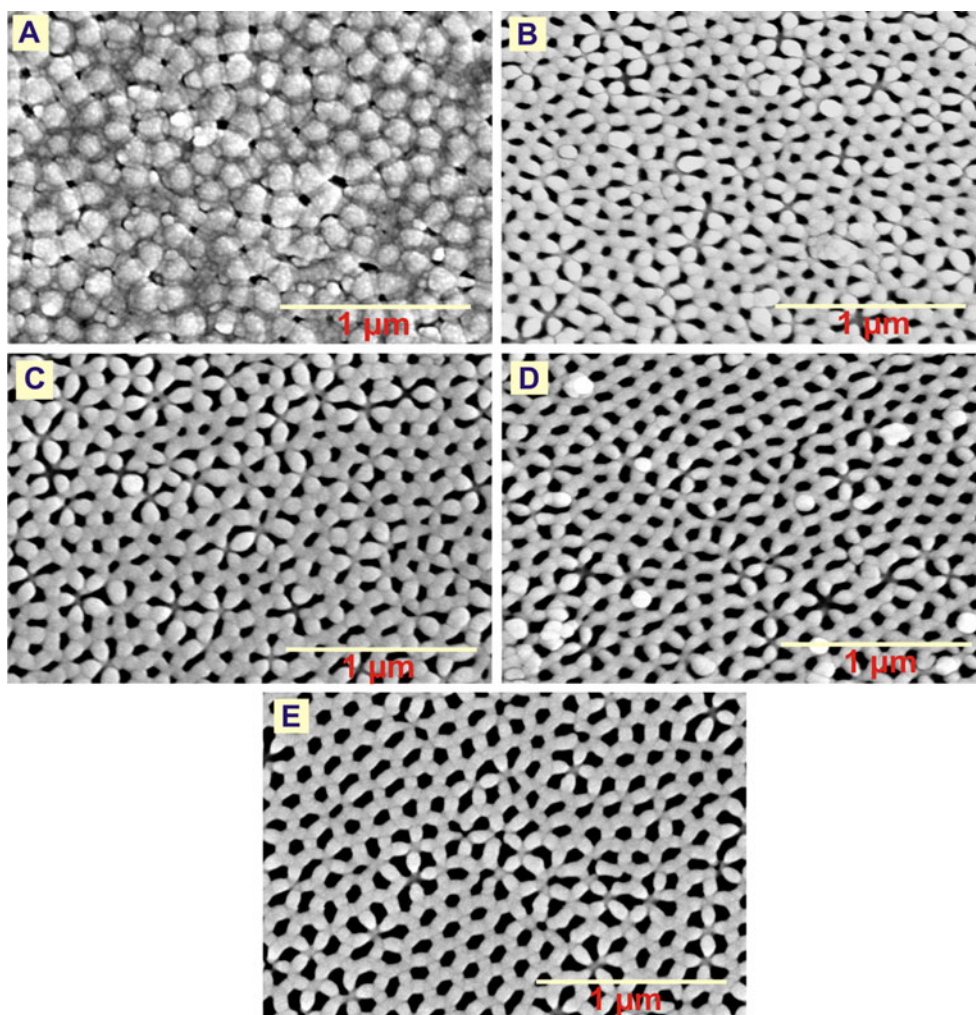

Fig. 6 FE-SEM top-view image of the AAO membrane formed by two-step anodization of the high-purity Al substrate in 0.3 M sulfuric acid at 25 V and 1 °C after 30 min of the pore opening/widening process carried out in 5 wt.% H_3PO_4 at 35 °C

shown in Fig. 8a and b, respectively. Also, the literature values of these parameters are illustrated as red lines. It is widely known that the interpore distance of the AAO membrane is linearly proportional to the anodizing potential with a proportionality constant of about 2.5 nm V^{-1}. The proportionality constant can slightly vary from 2.2 to 2.8 depending on anodizing conditions, especially anodizing electrolyte [21, 22, 39]. The excellent agreement between experimental and theoretical (literature) values can be observed in both cases. As can be expected, the interpore distance in AAOs and the pore density depend mainly on anodizing voltage, and the effect of other factors such as the type of electrolyte and temperature is negligible [12].

Conclusions

In summary, we have demonstrated the fabrication of through-hole nanopore membranes by two-step anodization of aluminum in sulfuric acid, oxalic acid, and phosphoric acid electrolytes. The anodizations were performed in 0.3 M

Fig. 7 FE-SEM images of the bottom side of the AAO membranes fabricated by anodizing of the high-purity Al substrate in 2 wt.% phosphoric acid at 175 V and 0 °C after pore opening/ widening in 10 wt.% H_3PO_4 at 45 °C. The duration of the pore opening was 30 min (**a**), 40 min (**b**), and 50 min (**c**)
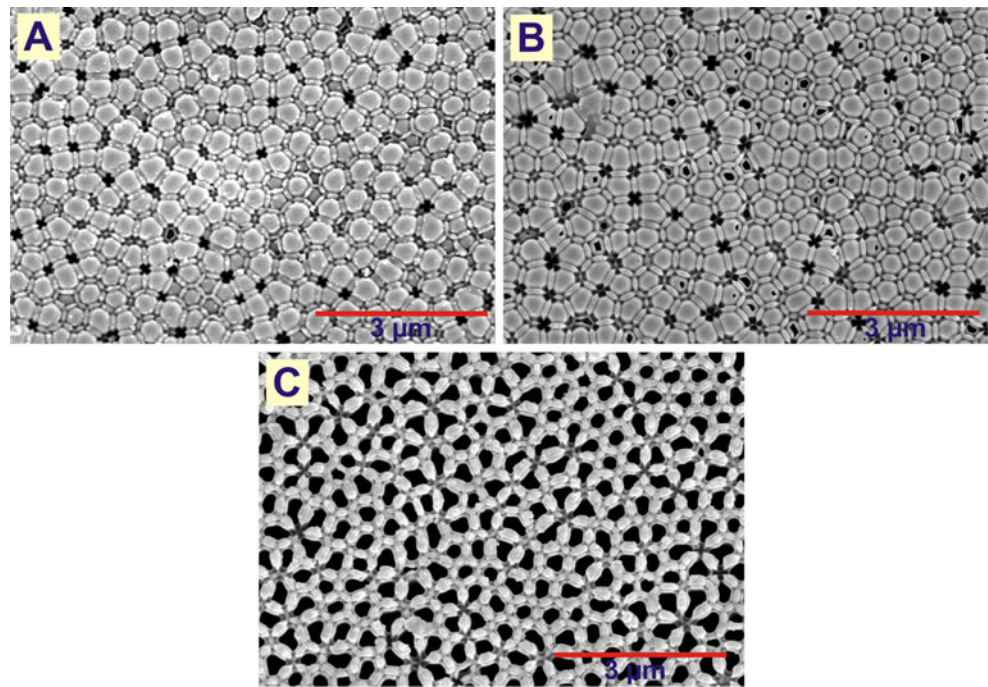

H_2SO_4 (25 V at 1 °C), $H_2C_2O_4$ (40 V at 1 °C or 45 V at 20 °C or 60 V at 20 °C), and a 2 wt.% phosphoric acid in methanol/water (1:4 vol.) solution (175 V at 0 °C). It was found that the rate of porous oxide growth depends on the type of anodizing electrolyte (the highest oxide growth rates were observed for anodizing in sulfuric acid, and the lowest oxide growth rates were recorded for anodic oxidation carried out in phosphoric acid), substrate purity (when the AA150 alloy was used as a starting material, the oxide growth rates were about 27% smaller), and anodizing voltage (an increase in anodizing potential results in a faster growth rate). Moreover, the oxide growth rate increases considerably with increasing anodizing temperature, and therefore, the time required for growth of thick AAO membranes in 0.3 M $H_2C_2O_4$ can be considerably shortened when anodization is carried out at 20 °C instead of 1 °C. It should be mentioned that although the pore order is worse

when the anodization is carried out at higher temperatures, it is still satisfactory and acceptable for using nanoporous membranes as templates for fabrication of nanowire arrays [18].

The barrier layer removal from the bottom side of AAO membranes was also investigated in detail. The procedure of wet chemical etching in phosphoric acid was carefully optimized for all studied membranes, and the effect of pore opening time on pore diameter was investigated. It was shown that the pore diameter can be tuned by careful adjustment of the etching conditions such as the electrolyte concentration and temperature. All structural features of nanoporous membranes together with anodizing and pore opening conditions are collected in Table 1. The rate of pore widening was also estimated for various temperatures of 5 wt.% H_3PO_4 used for dissolution of alumina formed in different electrolytes and anodizing potentials (Table 1).

Fig. 8 The influence of anodizing voltage on interpore distance (**a**) and pore density (**b**) of porous anodic alumina membranes formed by two-step anodizing of the high-purity Al substrate
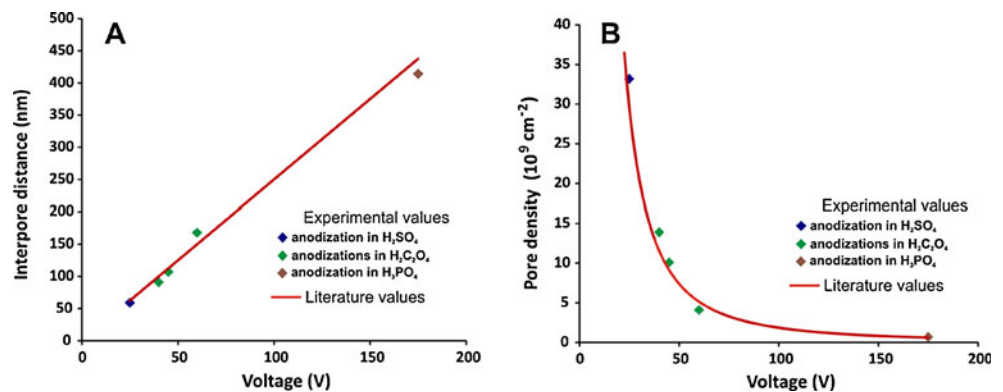
References

1. Bhushan B (ed) (2007) Springer handbook of nanotechnology, 2nd edn. Springer-Verlag, Berlin
2. Banerjee S, Dan A, Chakravorty D (2002) J Mater Sci 37:4261–4271
3. Fortuna SA, Li X (2010) Semicond Sci Technol 25:024005
4. Li Y, Qian F, Xiang J, Lieber CM (2006) Mater Today 9:18–27
5. Huang C, Hao Y (2009) Nanotechnology 20:445607
6. Bernholc J, Brenner D, Buongiorno Nardelli M, Meunier V, Roland C (2002) Annu Rev Mater Res 32:347–375
7. Polarz S, Smarsly B (2002) J Nanosci Nanotechnol 2:581–616
8. Weber J, Singhal R, Zekri S, Kumar A (2008) Int Mater Rev 53:235–255
9. She G, Mu L, Shi W (2009) Recent Pat Nanotechnol 3:182–191
10. Masuda H, Fukawa K (1995) Science 268:1466–1468
11. Masuda H, Satoh M (1996) Jpn J Appl Phys 35:L126–L129
12. Sulka GD (2008) In: Eftekhari A (ed) Nanostructured materials in electrochemistry. Wiley-VCH, Weinheim
13. Sulka GD, Zaraska L, Stępniowski WJ (2011) In: Nalwa HS (ed) Encyclopedia of nanoscience and nanotechnology, 2nd edn. American Scientific Publishers, CA
14. Sulka GD, Stroobants S, Moshchalkov V, Borghs G, Celis JP (2002) J Electrochem Soc 149:D97–D103
15. Sulka GD, Jaskuła M (2006) J Nanosci Nanotechnol 6:3803–3811
16. Sulka GD, Parkoła KG (2006) Thin Solid Films 515:338–345
17. Sulka GD, Stępniowski WJ (2009) Electrochim Acta 54:3683–3691
18. Sulka GD, Brzózka A, Zaraska L, Jaskuła M (2010) Electrochim Acta 55:4368–4376
19. Zaraska L, Sulka GD, Jaskuła M (2010) Surf Coat Technol 204:1729–1737
20. Zaraska L, Sulka GD, Jaskuła M (2009) J Phys Conf Ser 146:012020
21. O'Sullivan JP, Wood CG (1970) Proc R Soc Lond A 317:511–543
22. Nielsch K, Choi J, Schwirn K, Wehrspohn RB, Gösele U (2002) Nano Lett 2:677–680
23. Wood GC, O'Sullivan JP, Vaszko B (1968) J Electrochem Soc 115:618–620
24. Hwang SK, Jeong SH, Hwang HY, Lee OJ, Lee KH (2002) Kor J Chem Eng 19:467–473
25. Ba L, Li WS (2000) J Phys D Appl Phys 33:2527–2531
26. Xu T, Zangari G, Metzger RM (2002) Nano Lett 2:37–41
27. Lin MN, Lin MT, Liu CY, Lai MY, Liu NW, Peng CY, Wang HH, Wang YL (2005) Appl Phys Lett 87:173116
28. Lin MN, Liu CY, Liu NW, Lai MY, Peng CY, Wang HH, Wang YL, Lin MT (2006) Nanotechnology 17:315–319
29. Liu NW, Liu CY, Wang HH, Hsu CF, Lai MY, Chuang TH, Wang YL (2008) Adv Mater 20:2547–2551
30. Lillo M, Losic D (2009) Mater Lett 63:457–460
31. Yan B, Pham HTM, Ma Y, Zhuang Y, Sarro PM (2007) Appl Phys Lett 91:053117
32. Jiang X, Mishra N, Turner JN, Spencer MG (2007) IEEE Trans Nanotechnol 6:328–333
33. Xu WL, Chen H, Zheng MJ, Ding GQ, Shen WZ (2006) Optical Mater 28:1160–1165
34. Choi J, Sauer G, Nielsch K, Wehrspohn RB, Gösele U (2003) Chem Mater 15:776–779
35. Horcas I, Fernández R, Gómez-Rodríguez JM, Colchero J, Gómez-Herrero J, Baro AM (2007) Rev Sci Instrum 78:013705
36. Image J. National Institute of Mental Health. Bethesda, MD, USA, http://rsb.info.nih.gov/ij
37. Zaraska L, Sulka GD, Szeremeta J, Jaskuła M (2010) Electrochim Acta 55:4377–4386
38. Zaraska L, Sulka GD, Jaskuła M (2010) Surf Coat Technol 205:2432–2437
39. Keller F, Hunter MS, Robinson DL (1953) J Electrochem Soc 100:411–419